PAPER

Efficient catalytic oxidation of alcohol to carbonyl compounds over CoFe hydrotalcites†

W. Y. Zhou, J. G. Pan, Z. Wu, J. F. Qian, M. Y. He* and Q. Chen

A series of CO_3^{2-}–Co_xFe–LDHs (x = 2, 3, 4 and 5) compounds with different Co/Fe ratios have been prepared, characterized and introduced into the selective oxidation of alcohols by *tert*-butylhydroperoxide. The characterization including XRD, SEM, FTIR, TG/DTG, DR UV-vis, N_2 adsorption and XPS showed that the hydrotalcite structure was well formed with different Co/Fe ratios, and the ratio has significant influence on the materials' morphologies, physical properties and the composition of $Co^{2+}/Co^{3+}/Fe^{3+}$. The effects of varied reaction conditions on the catalytic oxidation have been investigated, and the results indicate that the co-existence of Co^{2+} and Co^{3+} is beneficial to the catalytic activity. Comparison experiments showed that substitution of Al with Fe could markedly increase the surface area of the material, and a synergistic effect might exist between Co and Fe in the CoFe hydrotalcites for the alcohol oxidation. In addition, the catalyst also exhibited excellent stability and catalytic performance in the oxidation of varied alcohols.

Introduction

Development of efficient catalysts for the selective oxidation of alcohol to carbonyl compounds is one of the important topics in synthetic and industrial chemistry, and has attracted much attention from chemists.[1] Varied catalysts have been developed for the transformation, and large progress has been made for the noble metal catalysts in liquid-phase oxidation of varied alcohols.[2] From the viewpoint of economy and sustainable chemistry, however, it is especially important to develop economical catalysts for the selective oxidation of alcohols, because noble metal catalysts are highly expensive and scarce.

To date, quite a lot of heterogeneous catalytic systems based on non-noble transition metals have also been reported, including Mn,[3] Ni,[4] Cr,[5] Co,[6] V (ref. 7) and Fe,[8] *etc.* However, most of these systems suffered from some drawbacks, including (i) low catalytic activity or selectivity; (ii) limited substrate scope; (iii) harsh reaction conditions and (iv) complicated preparation methods for the catalysts.

Cobalt-containing catalysts have been extensively studied, and some of them exhibited excellent results for given substrates. In the research of developing efficient and easily manufactured catalyst for the selective oxidation of alcohol, we have synthesized a series of hydrotalcites (LDH) containing cobalt.[6a,9] And we found that the surface basicity benefits to the selectivity of aldehyde for the primary alcohol oxidation, and the co-existence of Co^{2+} and

Co^{3+} can improve the catalytic activity in the reaction. Hydrotalcites, as a representative basic material, has been applied as catalysts in many reactions. Therefore, we envisioned that introduction of another transition metal into cobalt hydrotalcites might affect the composition of metallic ion with different valence, and improve the catalytic performance in the oxidation of alcohol.

In the preliminary study, we found that introduction of iron into the Co-containing hydrotalcites could markedly improve their catalytic activities in the oxidation of benzyl alcohol. We speculated that a synergistic effect between Co and Fe might exist in hydrotalcites compounds for the oxidation. Actually, the synergistic effect between Co and Fe in some kind of materials has been recently reported for electrochemical catalysis,[10] as well as the dehydrogenation of ethylbenzene[11] and CO oxidation.[12] To the best of our knowledge, however, the effect in hydrotalcites for the oxidation of alcohol has not been investigated.

On the basis of above analysis, in the present study, a series of CO_3^{2-}–Co_xFe–LDHs (x = 2, 3, 4 and 5) compounds with different Co/Fe ratios have been prepared, characterized and introduced into the selective oxidation of alcohols in liquid phase with *tert*-butylhydroperoxide (TBHP) as the oxidant. The effect of Co/Fe ratio on the physico-chemical properties of the catalysts and their catalytic properties in the oxidation of alcohol were investigated. In addition, the possible synergistic effect between Co and Fe in hydrotalcite for the reaction has also been discussed.

Results and discussion

Characterization of CO_3^{2-}–Co_xFe–LDHs samples

The powder XRD patterns for CO_3^{2-}–Co_xFe–LDHs with the Co/Fe ratio between 2 to 5 are depicted in Fig. 1. The patterns of all

Jiangsu Key Laboratory of Advanced Catalytic Materials and Technology, Changzhou University, Changzhou 213164, China. E-mail: hemy_cczu@126.com
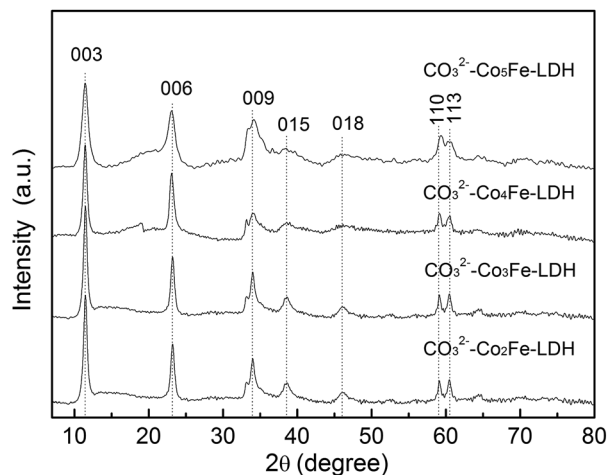
Fig. 1 XRD patterns of CO_3^{2-}–Co_xFe–LDHs.

the samples show characteristic LDH reflections (sharp and symmetrical for (003) and (006), broad and asymmetrical for (009), (015) and (018), respectively).[4a,13] Furthermore, the distinguishable reflections corresponding to planes (110) and (113) (recorded in the 2θ range 60–63°) were observed except for CO_3^{2-}–Co_5Fe–LDH, suggesting a well ordering of both the anions of the interlayer and the cations in the layers.[14] These results indicate that hydrotalcite structure formed for all the samples with different Co/Fe ratios. And the SEM images of CO_3^{2-}–Co_4Fe–LDH (Fig. 2) show that the synthesized sample formed plate-like agglomerated crystals, representing the character of layered materials.[15]

The IR spectra CO_3^{2-}–Co_4Fe–LDH and CO_3^{2-}–Co_4Al–LDH are depicted in Fig. S1,† it can be found that both LDHs show
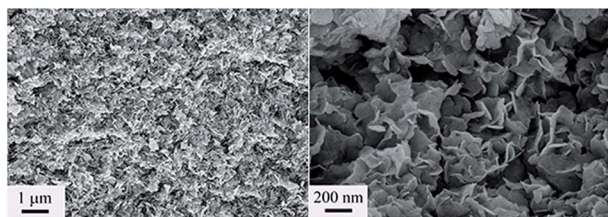
a broad and intense band at about 3500 cm^{-1}, which can be assigned to the –OH stretching vibration of layer hydroxyl groups and interlayer water molecules.[14b] These bands shift to lower frequencies when Al was replaced by Fe, indicating an increase of Me–OH bond strength.[16] The absorption at 1641 cm^{-1} is due to the bending vibration of water, and 1358 cm^{-1} to the carbonate anion in the interlayers for anti-symmetric stretching frequency. In the 400–1000 cm^{-1} region there are some bands related to vibrations cation–oxygen. The broaden appearance at 616 and 566 cm^{-1} are corresponding to the lattice vibration modes of Me–O in the LDH sheets. A broad peak at 757 cm^{-1} is associated with Al–OH. A shoulder at 985 cm^{-1} for Al–OH deformation increases to 1004 cm^{-1} in CO_3^{2-}–Co_4Fe–LDH may be affected by the substitution of Al with Fe.

TG/DTG curves of CoFe hydrotalcites show three main stages of weight loss around 50–170 °C, 170–250 °C and 250–450 °C (Fig. S2†). The first stage corresponds to the loss of physically adsorbed water on the external surface, whereas the next stage results from the evaporation of water molecules in the interlayer space of CoFe hydrotalcites. The last stage can be put down to the dehydration of hydroxyl groups on the brucite layers and also the loss of CO_2 from the interlayers.[17]

For the purpose of exploring the textural parameters of CoFe hydrotalcites with different Co/Fe ratios, nitrogen sorption measurement was carried out. The corresponding pore size distribution curves for these CoFe hydrotalcites are presented in Fig. S3.† It can be observed that the isotherm for these samples are all type IV according to the IUPAC classification, conforming the mesoporous structure of the materials. On the other hand, for all the samples, H3 type hysteresis loops were observed, indicating aggregates of plate-like particles containing slit-shaped pores formed under the synthesis.[18]

Table 1 summarizes the data of the surface areas, pore volumes and pore sizes of these samples. It is observed that Co/Fe ratio slightly affect the data. However, compared with CO_3^{2-}–Co_4Al–LDH, the BET surface areas of these samples increase, whereas these average pore diameter and pore volume decrease. Changes in the porosity characteristics may be attributed to the alteration of the microscopic morphology due to the presence of different cations within the structure, in consistent with the previously reported results.[18,19] The increasement may benefit to the catalytic performance.

Fig. 2 SEM images of CO_3^{2-}–Co_4Fe–LDH.

Table 1 Sample notation and chemical compositions of CO_3^{2-}–Co_xFe–LDHs

Sample	Weight content (%)		Co/Fe[a]	S_{BET} (m^2 g^{-1})	Pore volume (cm^3 g^{-1})	Average pore diameter (nm)	Co^{3+b} (%)	Co^{2+b} (%)	Fe^{3+b} (%)
	Co	Fe							
CO_3^{2-}–Co_2Fe–LDH	30.3	15.4	1.9 : 1	112	0.19	9.3	1.4	14.1	2.4
CO_3^{2-}–Co_3Fe–LDH	35.6	12.1	2.8 : 1	191	0.26	8.2	2.2	14.4	1.7
CO_3^{2-}–Co_4Fe–LDH	36.9	9.6	3.6 : 1	131	0.27	10.5	1.6	14.7	1.1
CO_3^{2-}–Co_5Fe–LDH	37.5	7.6	4.7 : 1	158	0.25	8.8	2.0	14.3	1.0
CO_3^{2-}–Co_4Al–LDH	43.2	11.3	3.8 : 1	52	0.39	30.0	1.4	18.4	—

[a] Analyzed by ICP. [b] Based on the analysis of XPS.

DR UV-vis spectroscopy is an effective method to detect prepared CO_3^{2-}–Co_xFe–LDHs with different Co/Fe ratios. Fig. 3 shows the DR UV-vis spectra of the various materials. Inspection of the spectra reveals that, the appearance of an absorption bands at 255 nm is assigned to tetra-coordinated Fe^{3+} species.[20] And the band centered to 531 nm (λ_3) can be related to transition $^4T_{1g}(F) \rightarrow {}^4T_{1g}(P)$ of $[Co(H_2O)_6]^{2+}$.[21] As the increasing of the Co/Fe ratio, the band for Fe^{3+} decreases, and the darkening of the color of the Co_5Fe–LDH sample to beige supposes a partial oxidation of Co^{2+} to Co^{3+} ions. This supposition is supported by the increased band at 624 nm, which can be ascribed to d–d transitions in low spin Co^{3+} (OH) species ($^1A_{g_{1g}} \rightarrow {}^1T_{1g}$), in accordance to the report by Gabrovska[22] and Khassin.[23]

It is well known that the catalytic activity of the materials containing transition metals is associated with the oxidation states of the transition metals. The detailed chemical and electronic states of the CO_3^{2-}–Co_xFe–LDHs were further determined by XPS, which gave information about surface and near-surface ions. The XPS survey spectra (not shown) of all the samples show typical signals for the Co, Fe, C, and O elements. The high-resolution XPS spectra of the Fe 2p can be fitted by four peaks (Fig. S4†), and binding energies of Fe $2p_{1/2}$ (ca. 726 eV) and Fe $2p_{3/2}$ (ca. 713 eV) are identified, referring to Fe(III).[24] After the peak fitting procedure for the Co 2p spectra (Fig. 4), two kinds of cobalt species are observed, containing the Co^{2+} at binding energies of about 781.3 eV and 797.3 eV, and Co^{3+} at binding energies of about 780.6 and 795.6 eV.[25] These results show that cobalt existed as multiple valence state in CO_3^{2-}–Co_xFe–LDHs nanosheets, indicating that partial oxidation of Co^{2+} ions was occurring during the synthesis procedure due to the thermodynamically favored oxidation of Co^{2+} to Co^{3+} ions.[26] Large content of cobalt in a sample can also result in the oxidation,[27] which has been verified by the CO_3^{2-}–Co_4Al–LDH samples (Fig. S5†). In addition, the mole ratio of Co^{2+}/Co^{3+} on the surface can be quantitatively calculated based on the two spin–orbit doublets. Therefore, the content of these metal ions, including Co^{2+}, Co^{3+} and Fe^{3+} can be calculated by combining

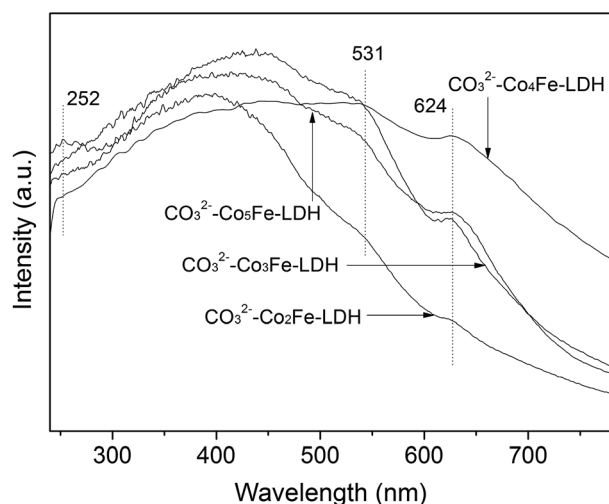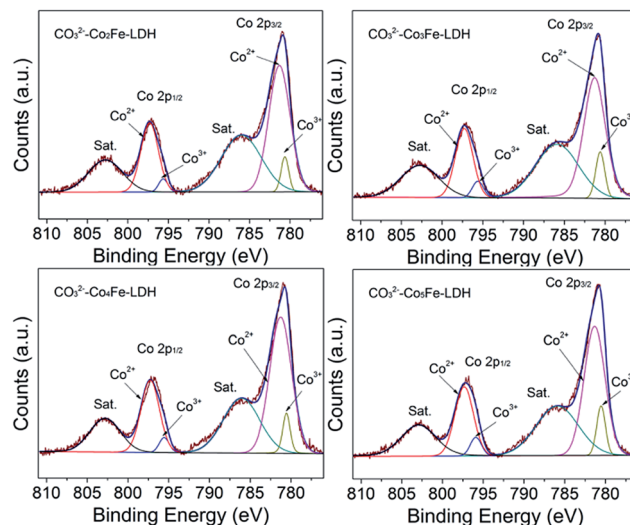**Fig. 4** The Co 2p XPS spectra of CO_3^{2-}–Co_xFe–LDHs (x = 2, 3, 4 and 5).

the above results and XPS spectra (Table 1). The content of Co^{3+} in CO_3^{2-}–Co_4Al–LDH is lower than that of CO_3^{2-}–Co_4Fe–LDH (Table 1), indicating that the substitution of Al by Fe may also affect the composition of Co^{2+} and coordination states of incorporated cobalt and iron species in Co^{3+}. The irregular distribution of Co^{2+} and Co^{3+} from the XPS spectra analysis may be due to the influence of multi-factors. Summary, the Co^{2+} is partly transformed into Co^{3+} in the prepared CoFe hydrotalcites, in accordance with the results of the DR UV-vis.

Catalytic activity of CO_3^{2-}–Co_xFe–LDHs samples

In the present investigation, the oxidation of benzyl alcohol was examined as a standard substrate catalyzed by CO_3^{2-}–Co_xFe–LDHs samples using TBHP as the oxidant. The effect of solvent on the catalytic oxidation under CO_3^{2-}–Co_4Fe–LDH was firstly investigated, and the main data are summarized in Table 2 (the GC graph analysis can be found in Fig. S6†). The main by-product of the oxidation was benzoic acid and no ester was detected. The results indicate that the nature of the solvent has a strong influence on the alcohol conversion and the product selectivity. The conversion of alcohol increased with increasing polarity of the solvent, whereas the influence of the polarity on

Table 2 Effect of solvent on the oxidation of benzyl alcohol[a]

Entry	Solvent	C^b (%)	S^c (%)
1	Acetonitrile	60.1	86.0
2	Dimethyl sulfoxide	68.9	64.3
3	Hexane	23.7	95.2
4	Dichloromethane	39.9	89.6
5	Ethyl acetate	35.8	82.3

[a] Reaction conditions: benzyl alcohol 5 mmol; CO_3^{2-}–Co_4Fe–LDH 54 mg; TBHP 7.5 mmol; 60 °C; 2 h. [b] Conversion of benzyl alcohol. [c] Selectivity of benzaldehyde.

Fig. 3 The DR UV-vis spectra of CO_3^{2-}–Co_xFe–LDHs.

the selectivity of aldehyde was complex. This may be attributed to the fact that a polar solvent is preferred to form a polar product. Among these solvents, acetonitrile, possessing appropriate polarity exhibited the highest yield and selectivity of benzaldehyde.

As to the reaction temperature, it is observed that (Fig. 5) low reaction temperature significantly reduced the catalytic performance. The conversion of benzyl alcohol increased rapidly with the reaction temperature increasing, whereas the selectivity towards benzaldehyde decreased sharply when the temperature was higher than 60 °C. Higher reaction temperature favors the over oxidation of benzaldehyde to benzoic acid. The yield of benzaldehyde reached to 51.7% when the reaction temperature was 60 °C under the selected reaction conditions.

In this study, the influence of catalyst amount on the benzyl alcohol oxidation has also been investigated, and the results are shown in Fig. 6A. The conversion of alcohol increased from 48.4% to 73.2% when the catalyst increased from 27 mg to 108 mg, whereas the selectivity of benzaldehyde decreased from 90.3% to 45.5%. The selectivity of benzoic acid increased upon increasing catalyst dosage (not shown), indicating that the catalyst dosage plays a crucial role in converting aldehyde to benzoic acid. The same pattern was found in the influence of the ratio of TBHP to benzyl alcohol (Fig. 6B). The highest yield of aldehyde was obtained when 1.5 equivalent of TBHP was used, while increasing the amount resulted in a significantly decrease of the selectivity.

With the optimized conditions in hand, the effect the Co/Fe ratio on the catalytic performance was then discussed. The blank experiment (Table 3, entry 1) exhibited that the prepared samples performed as the catalyst in the oxidation. The ratio of Co/Fe also exhibited a significant effect on the catalytic performance (Table 3), the conversion of benzyl alcohol and the yield of benzaldehyde reached the highest when the ratio was 4. The results may be mainly related to the composition of Co^{2+}, Co^{3+} and Fe^{3+}, rather than the S_{BET}, pore volume and pore size. In the

Fig. 6 Effects of catalyst amount (A) and TBHP/alcohol (B) on the oxidation of benzyl alcohol (benzyl alcohol 5 mmol; acetonitrile 6 mL; 60 °C; 2 h. (A) TBHP 7.5 mmol; (B) CO_3^{2-}–Co_4Fe–LDH 54 mg).

presence of redox metals, TBHP is probably decomposed through a Haber–Weiss mechanism involving monoelectronic transfer. For the redox pairs Co(III)/Co(II) involved in this case, the mixed state of cobalt ions should be beneficial to the catalytic activity of the prepared samples.

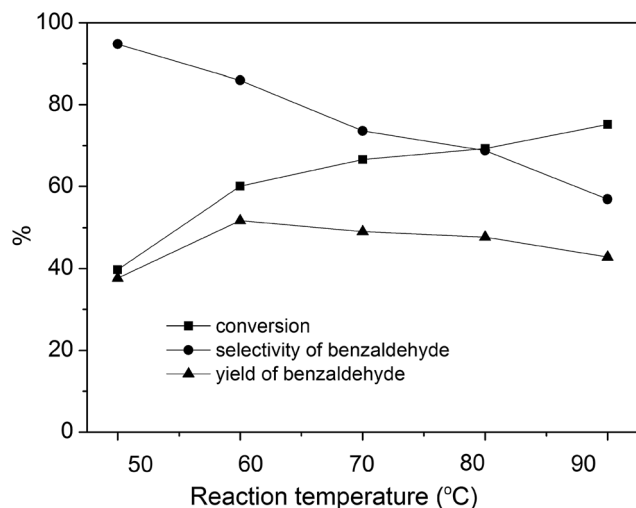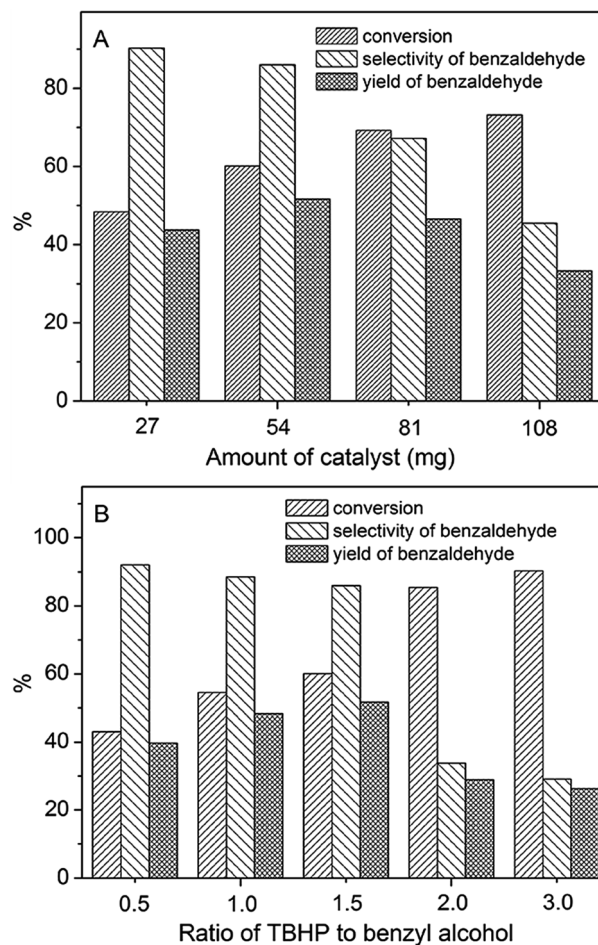Fig. 5 Effect of temperature on the catalytic oxidation of benzyl alcohol (benzyl alcohol 5 mmol; acetonitrile 6 mL; CO_3^{2-}–Co_4Fe–LDH 54 mg; TBHP 7.5 mmol; 2 h).

Table 3 Catalytic oxidation of benzyl alcohol under different conditions[a]

Entry	Catalyst	C^b (%)	S^c (%)
1	No catalyst	21.0	98
2	CO_3^{2-}–Co_2Fe–LDH	40.8	95.4
3	CO_3^{2-}–Co_3Fe–LDH	47.6	89.2
4	CO_3^{2-}–Co_4Fe–LDH	60.1	86.0
5	CO_3^{2-}–Co_5Fe–LDH	56.0	87.2
6	CO_3^{2-}–Co_4Al–LDH	29.6	90.5
7	CO_3^{2-}–Mg_4Fe–LDH	13.1	100
8	CO_3^{2-}–Co_4Fe–LDH[3rd]	59.4	87.1
9	CO_3^{2-}–Co_4Fe–LDH[5th]	59.9	85.2
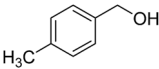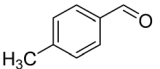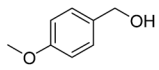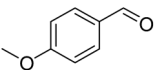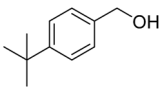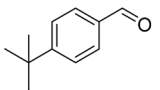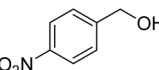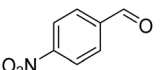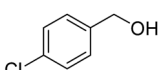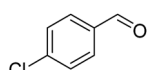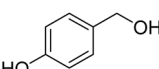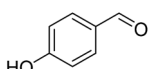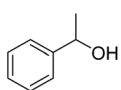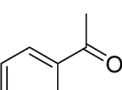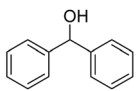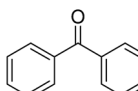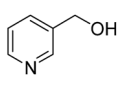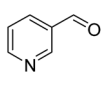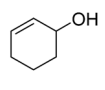
[a] Reaction conditions: benzyl alcohol 5 mmol; acetonitrile 6 mL; catalyst 54 mg; TBHP 7.5 mmol; 60 °C; 2 h. [b] Conversion of benzyl alcohol. [c] Selectivity of benzaldehyde.

To find the probable synergistic effect between Co and Fe in the structure, some controlled experiments were performed. Firstly, CO_3^{2-}–Co_4Al–LDH was introduced into the reaction. The result in Table 3 (entry 6) shows that the conversion of benzyl alcohol significantly increased from 29.6% to 60.1%, indicating that Fe in the structure could efficiently improve the catalytic activity. This phenomenon may be partly ascribed to the changes of the catalysts' physical and chemical properties including the S_{BET}, because the S_{BET} markedly increased after replacing Al by Fe (Table 1). Then CO_3^{2-}–Mg_4Fe–LDH (XRD pattern was shown in Fig. S7†) was also prepared by the same method and tested in the reaction. Interestingly, the catalyst could not accelerate the oxidation, but hamper it (Table 3, entry 7). These results indicate that synergistic effect may exist between Co and Fe in the catalytic oxidation of alcohol under CoFe hydrotalcites.

In order to assess the stability of the catalysts, the catalyst was separated from the reaction mixture after each experiment by filtration, washed with the acetonitrile and dried. The results in Table 3 (entries 8 and 9) showed that the prepared catalyst could be reused at least five times without changes of catalytic activity, indicating that the synthesized CO_3^{2-}–Co_xFe–LDHs were stable under the reaction conditions. The ICP analysis of the recycled catalyst showed that Co and Fe 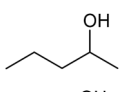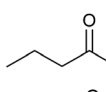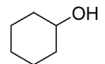contents were 36.8% and 9.6%, respectively, whereas no Co or Fe ions was detected in the filtrate. These results indicated that almost no leaching of metal ion after catalytic reaction. The XRD pattern (Fig. S8†) and SEM images (Fig. S9†) of the recycled catalyst

Table 4 Catalytic oxidation of varied alcohols under CO_3^{2-}–Co_4Fe–LDH[a]

Entry	Substrate	Product	C^b (%)	S^c (%)	t^d (h)
1			68.8	63.2	1
2			79.6	69.0	1.5
3			62.1	61.4	1
4			78.0 (18.8)[e]	84.8 (>99)[e]	3
5			53.1	84.5	2
6			0	—	10
7			>99	>99	3
8			>99	>99	0.5
9			>99	>99	12
10			84.6	85.4	24
11			92.2	>99	30
12			81.5	>99	24

[a] Reaction conditions: substrate 5 mmol; acetonitrile 6 mL; CO_3^{2-}–Co_4Fe–LDH 54 mg; TBHP 7.5 mmol; 60 °C. [b] Conversion of benzyl alcohol. [c] Selectivity of benzaldehyde. [d] Reaction time. [e] The results obtained at 1 h.

show that the structure of the catalyst did not change during the catalytic oxidation. In addition, the crystallinity of the recycled CoFe hydrotalcite seems improved, which may be due to the solvothermal effect. Being heated in the reaction system may benefit to the crystallinity of hydrotalcite samples.

In summary, CoFe hydrotalcites has been proved to be an efficient catalyst for the oxidation of benzyl alcohol under the selected conditions. Mobley et al.[28] have comprehensively reviewed the hydrotalcites catalysts for the oxidation of alcohol using TBHP. Compared with the results summarized in the literature, the prepared CO_3^{2-}–Co_4Fe–LDH exhibited even higher conversion of benzyl alcohol and yield of benzaldehyde.

To further elucidate the scope of substrate, various alcohols have been introduced into the reaction system. In general, when the analogs of benzyl alcohol were used in the reaction, the moderate yields were obtained (Table 4, entries 1–5) except 4-hydroxybenzyl alcohol (entry 6), and the main by-products were the corresponding acid. From the reaction time needed for these substrates with different substituents, it is ease to conclude that electronic variation on the aromatic substituents has some effects on the activity. Benzyl alcohols substituted with electron-donating groups such as $-CH_3$, $-OCH_3$ and $-C(CH_3)_3$ (Table 4, entries 1–3) exhibited higher activity as compared to those with electron-withdrawing groups (Table 4, entries 4 and 5). No reaction was observed for 4-hydroxybenzyl alcohol, indicating that free radical formed in the reaction, which is consistent with the reported results.[29] For the oxidation of secondary alcohol, excellent yields (Table 4, entries 7 and 8) were obtained, indicating the high catalytic activity of the as-synthesized CoFe hydrotalcites. On the other hand, the catalytic system was also very efficient for the aromatic alcohols with hetero atoms (Table 4, entry 9) and aliphatic alcohols (Table 4, entries 10–12).

Conclusions

In the present work, CO_3^{2-}–Co_xFe–LDHs samples with different Co/Fe ratio by a coprecipitation method were prepared and investigated in the selective oxidation of various alcohols to aldehyde or ketone. The results showed that replacing of Al by Fe can effectively improve the catalytic activities of Co-containing hydrotalcites, which may correlate to the coexistence of Co^{2+}, Co^{3+} and Fe^{3+}, and a proper composition of them. A synergistic effect between Co and Fe in the catalytic oxidation of alcohol was observed. Substitution of Al with Fe could markedly increase the surface area of the material and accelerate the transformation of Co^{2+} to Co^{3+} in the CoFe hydrotalcites. The prepared catalysts also exhibited efficient catalytic activities for varied alcohols and high selectivity of aldehyde for primary alcohols.

Experimental

All reagents and solvents were of analytical grade and were obtained commercially. No impurities were found in all the substrates by GC-MS analysis before use.

Preparation of catalysts

CO_3^{2-}–Co_xFe–LDHs with different Co/Fe ratio ($x = 2, 3, 4$ and 5) were synthesized by a coprecipitation method. In a typical procedure, 0.04 mol of $Co(NO_3)_2 \cdot 6H_2O$ and 0.02 mol of $Fe(NO_3)_3 \cdot 9H_2O$ were dissolved in 120 mL deionized water to form solution A, and solution B was prepared by dissolving 0.067 mol of Na_2CO_3 and 0.2 mol of NaOH in 120 mL deionized water. These two solutions were added dropwise with stirring to 100 mL deionized water at 60 °C while the pH was maintained between 9.5–10. After that, the resulting slurry was stirred for another 30 min and then digested at 80 °C for 24 h. The precipitate was washed with deionized water until the pH of the filtrate was around 7.0. The solid product named CO_3^{2-}–Co_2Fe–LDH was obtained after being dried in an oven at 100 °C for 12 h. Other samples with different Co/Fe ratios were synthesized via similar method.

Characterization of catalysts

Powder X-ray diffraction (XRD) patterns of these prepared samples were obtained from a Rigaku D/max 2500 PC X-ray diffractometers with Cu-Kα (1.5402 Å) radiation at 10 min^{-1}. Inductively coupled plasma analysis (ICP) was used to analyze the compositions of samples in a Varian Vista-AX device. Diffuse reflectance ultraviolet visible spectra (DR UV-vis) were recorded in a Perkin-Elmer Lambda 35 spectrophotometer, using $BaSO_4$ as a reference. Porosity and surface area studies were performed on a micromeritics ASAP2010C apparatus, using nitrogen as the absorbate at liquid nitrogen temperature (−196 °C). The surface area was calculated using the BET method and the pore size distributions were deduced from the adsorption branches of the isotherms using the BJH method. X-ray photoelectron spectroscopy (XPS) measurements were performed with a PHI Quantera II instrument using non-monochromatized Mg Kα radiation at a pass energy of 50 eV and an electron take off angle of 60°. The correction of binding energy was performed by using the C 1s peak of carbon at 285 eV as reference. The IR spectra were obtained on a Nicolet PROTÉGÉ 460 FTIR spectrometer in the region 4000–400 cm^{-1} using KBr pellets. And a JEOL JSM-6360LA scanning electron microscope was used for the scanning electron microscopy (SEM) study of the samples.

Reaction procedure for benzyl alcohol oxidation

The oxidation of benzyl alcohol was carried out in a 25 mL two-neck-flask with reflux condenser and magnetically stirred heated in an oil bath. Acetonitrile (solvent, 6 mL), catalyst (54 mg) and 5 mmol benzyl alcohol were introduced into the flask and magnetically stirred at 60 °C, followed by dropwise addition of 7.5 mmol of TBHP (dried and dissolved in acetonitrile). The product samples were drawn at regular time intervals and analyzed using a GC-MS (Shimadzu GCMS-2010) and a gas chromatography (Shimadzu GC-2010AF) with Chromopak capillary column and FID detector. The conversion, yield of benzaldehyde and selectivity presented here are based on the GC calculations using cyclohexane as the internal standard reference compound. Moreover, for the test of reusability, the used catalyst was

removed from the reaction mixture by filtration and washed with acetonitrile and dried in an oven at 100 °C for 12 h.

Acknowledgements

Notes and references

1 (a) N. Gunasekaran, *Adv. Synth. Catal.*, 2015, **357**, 1990–2010; (b) T. Mallat and A. Baiker, *Chem. Rev.*, 2004, **104**, 3037–3058; (c) J. Luo, H. Yu, H. J. Wang, H. H. Wang and F. Peng, *Chem. Eng. J.*, 2014, **240**, 434–442.

2 (a) H. W. Wang, C. L. Wang, H. Yan, H. Yi and J. L. Lu, *J. Catal.*, 2015, **324**, 59–68; (b) A. Noujima, T. Mitsudome, T. Mizugaki, K. Jitsukawa and K. Kaneda, *Angew. Chem., Int. Ed.*, 2011, **50**, 2986–2989; (c) X. M. Huang, X. G. Wang, X. S. Wang, X. X. Wang, M. W. Tan, W. Z. Ding and X. G. Lu, *J. Catal.*, 2013, **301**, 217–226; (d) K. Yamaguchi, J. W. Kim, J. L. He and N. Mizuno, *J. Catal.*, 2009, **268**, 343–349.

3 (a) A. R. Judy-Azar and S. Mohebbi, *J. Mol. Catal. A: Chem.*, 2015, **397**, 158–165; (b) G. Wu, Y. Gao, F. W. Ma, B. H. Zheng, L. G. Liu, H. Y. Sun and W. Wu, *Chem. Eng. J.*, 2015, **271**, 14–22; (c) Y. C. Son, V. D. Makwana, A. R. Howell and S. L. Suib, *Angew. Chem., Int. Ed.*, 2001, **40**, 4280–4283.

4 (a) B. M. Choudary, M. L. Kantam, A. Rahman, C. V. Reddy and K. K. Rao, *Angew. Chem., Int. Ed.*, 2001, **40**, 763–766; (b) C. L. Li, H. Kawada, X. Y. Sun, H. Y. Xu, Y. Yoneyama and N. Tsubaki, *ChemCatChem*, 2011, **3**, 684–689.

5 (a) A. S. Burange, R. V. Jayaram, R. Shukla and A. K. Tyagi, *Catal. Commun.*, 2013, **40**, 27–31; (b) K. Li, D. Zhou, J. J. Deng, X. H. Lu and Q. H. Xia, *J. Mol. Catal. A: Chem.*, 2014, **387**, 31–37.

6 (a) W. Y. Zhou, J. Liu, J. G. Pan, F. A. Sun, M. Y. He and Q. Chen, *Catal. Commun.*, 2015, **69**, 1–4; (b) V. R. Choudhary, D. K. Dumbre, B. S. Uphade and V. S. Narkhede, *J. Mol. Catal. A: Chem.*, 2004, **215**, 129–135; (c) A. S. Burange, S. R. Kale, R. Zboril, M. B. Gawande and R. V. Jayaram, *RSC Adv.*, 2014, **4**, 6597–6601.

7 (a) V. Mahdavi and S. Soleimani, *Mater. Res. Bull.*, 2014, **51**, 153–160; (b) G. C. Behera and K. M. Parida, *Appl. Catal., A*, 2012, **413**, 245–253.

8 L. L. Geng, B. Zheng, X. Wang, W. X. Zhang, S. J. Wu, M. J. Jia, W. F. Yan and G. Liu, *ChemCatChem*, 2016, **8**, 805–811.

9 W. Y. Zhou, P. Tian, F. A. Sun, M. Y. He and Q. Chen, *J. Catal.*, 2016, **335**, 105–116.

10 (a) M. S. Burke, M. G. Kast, L. Trotochaud, A. M. Smith and S. W. Boettcher, *J. Am. Chem. Soc.*, 2015, **137**, 3638–3648; (b) C. X. Xiao, X. Y. Lu and C. Zhao, *Chem. Commun.*, 2014, **50**, 10122–10125.

11 B. B. Tope, R. J. Balasamy, A. Khurshid, L. A. Atanda, H. Yahiro, T. Shishido, K. Takehira and S. S. Al-Khattaf, *Appl. Catal., A*, 2011, **407**, 118–126.

12 (a) A. Biabani-Ravandi and M. Rezaei, *Chem. Eng. J.*, 2012, **184**, 141–146; (b) A. Biabani-Ravandi, M. Rezaei and Z. Fattah, *Chem. Eng. Sci.*, 2013, **94**, 237–244.

13 (a) Z. Y. Sun, C. G. Lin, J. Y. Zheng, L. Wang, J. W. Zhang, F. L. Xu and J. Hou, *Mater. Lett.*, 2013, **113**, 83–86; (b) A. Romero, M. Jobbígy, M. Laborde, G. Baronetti and N. Amadeo, *Catal. Today*, 2010, **149**, 407–412.

14 (a) P. Benito, F. M. Labajos and V. Rives, *J. Solid State Chem.*, 2006, **179**, 3784–3797; (b) L. L. Wang, B. Li, Z. Q. Hu and J. J. Cao, *Appl. Clay Sci.*, 2013, **72**, 138–146.

15 (a) S. Abelló, F. Medina, D. Tichit, J. Pérez-Ramírez, X. Rodríguez, J. E. Sueirasa, P. Salagrea and Y. Cesterosa, *Appl. Catal., A*, 2005, **281**, 191–198; (b) H. C. Greenwell, P. J. Holliman, W. Jones and B. V. Velasco, *Catal. Today*, 2006, **114**, 397–402.

16 N. V. Kosova, E. T. Devyatkina and V. V. Kaichev, *J. Power Sources*, 2007, **174**, 735–740.

17 (a) C. Zhang, S. G. Yang, H. Z. Chen, H. He and C. Sun, *Appl. Surf. Sci.*, 2014, **301**, 329–337; (b) K. Y. Ma, J. P. Cheng, J. Zhang, M. Li, F. Liu and X. B. Zhang, *Electrochim. Acta*, 2016, **198**, 231–240; (c) S. V. Prasanna, P. V. Kamath and C. Shivakumara, *Mater. Res. Bull.*, 2007, **42**, 1028–1039.

18 E. M. Seftel, M. Niarchos, N. Vordos, J. W. Nolan, M. Mertens, A. C. Mitropoulos and E. F. Vansant, *Microporous Mesoporous Mater.*, 2015, **203**, 208–215.

19 E. M. Seftel, E. Popovici, M. Mertens, G. Van Tendeloo, P. Cool and E. F. Vansant, *Microporous Mesoporous Mater.*, 2008, **111**, 12–17.

20 K. M. Parida and S. K. Dash, *J. Hazard. Mater.*, 2010, **179**, 642–649.

21 K. Gailey and R. Palmer, *Chem. Phys. Lett.*, 1972, **13**, 176–180.

22 M. Gabrovska, R. Edreva-Kardjieva, K. Tenchev, P. Tzvetkov, A. Spojakina and L. Petrov, *Appl. Catal., A*, 2011, **399**, 242–251.

23 A. A. Khassin, V. F. Anufrienko, V. N. Ikorskii, L. M. Plyasova, G. N. Kustova, T. V. Larina, I. Y. Molina and V. N. Parmon, *Phys. Chem. Chem. Phys.*, 2002, **4**, 4236–4243.

24 (a) M. A. Oliver-Tolentino, J. Vazquez-Samperio, A. Manzo-Robledo, R. D. G. Gonzalez-Huerta, J. L. Flores-Moreno, D. Ramírez-Rosales and A. Guzman-Vargas, *J. Phys. Chem. C*, 2014, **118**, 22432–22438; (b) Y. L. Wang, F. J. Li, S. G. Dong, X. W. Liu and M. G. Li, *J. Colloid Interface Sci.*, 2016, **467**, 28–34.

25 (a) M. Prabu, K. Ketpang and S. Shanmugam, *Nanoscale*, 2014, **6**, 3173–3181; (b) J. Jiang, A. L. Zhang, L. L. Li and L. H. Ai, *J. Power Sources*, 2015, **278**, 445–451.

26 (a) J. Pérez-Ramírez, G. Mul, F. Kapteijn and J. Moulijn, *Mater. Res. Bull.*, 2001, **36**, 1767–1775; (b) M. Ulibarri, J. Fernández, F. Labajos and V. Rives, *Chem. Mater.*, 1991, **3**, 626–630.

27 A. Corma and H. Garcia, *Chem. Soc. Rev.*, 2008, **37**, 2096–2126.

28 J. K. Mobley and M. Crocker, *RSC Adv.*, 2015, **5**, 65780–65797.

29 J. Taghavimoghaddam, G. P. Knowles and A. L. Chaffee, *J. Mol. Catal. A: Chem.*, 2013, **379**, 277–286.